

Influence of sub-bandgap illumination on space charge distribution in CdZnTe detector

Rongrong Guo(郭榕榕), Jinhai Lin(林金海), Lili Liu(刘莉莉), Shiwei Li(李世韦), Chen Wang(王尘), Feibin Xiong(熊飞兵), and Haijun Lin(林海军)

Citation: Chin. Phys. B, 2021, 30 (**3**): 036101. DOI: 10.1088/1674-1056/abc67e
Journal homepage: http://cpb.iphy.ac.cn; http://iopscience.iop.org/cpb

What follows is a list of articles you may be interested in

CdS/Si nanofilm heterojunctions based on amorphous silicon films: Fabrication, structures, and electrical properties

Yong Li(李勇), Peng-Fei Ji(姬鹏飞), Yue-Li Song(宋月丽), Feng-Qun Zhou(周丰群), Hong-Chun Huang(黄宏春), and Shu-Qing Yuan(袁书卿)

Chin. Phys. B, 2021, 30 (**2**): 026101. DOI: 10.1088/1674-1056/abc15e

Tunable electronic structures of germanane/antimonene van der Waals heterostructures using an external electric field and normal strain

Xing-Yi Tan(谭兴毅), Li-Li Liu(刘利利), Da-Hua Ren(任达华)

Chin. Phys. B, 2020, 29 (**7**): 076102. DOI: 10.1088/1674-1056/ab8a39

Improved carrier transport in Mn:ZnSe quantum dots sensitized La-doped nano-TiO_2 thin film

Shao Li(李绍), Gang Li(李刚), Li-Shuang Yang(杨丽爽), Kui-Ying Li(李葵英)

Chin. Phys. B, 2020, 29 (**4**): 046104. DOI: 10.1088/1674-1056/ab7742

Growth and doping of bulk GaN by hydride vapor phase epitaxy

Yu-Min Zhang(张育民), Jian-Feng Wang(王建峰), De-Min Cai(蔡德敏), Guo-Qiang Ren(任国强), Yu Xu(徐俞), Ming-Yue Wang(王明月), Xiao-Jian Hu(胡晓剑), Ke Xu(徐科)

Chin. Phys. B, 2020, 29 (**2**): 026104. DOI: 10.1088/1674-1056/ab65b9

Radiation-induced 1/*f* noise degradation of PNP bipolar junction transistors at different dose rates

Qi-Feng Zhao(赵启凤), Yi-Qi Zhuang(庄奕琪), Jun-Lin Bao(包军林), Wei Hu(胡为)

Chin. Phys. B, 2016, 25 (**4**): 046104. DOI: 10.1088/1674-1056/25/4/046104

Influence of sub-bandgap illumination on space charge distribution in CdZnTe detector*

Rongrong Guo(郭榕榕)†, Jinhai Lin(林金海), Lili Liu(刘莉莉), Shiwei Li(李世韦), Chen Wang(王尘), Feibin Xiong(熊飞兵), and Haijun Lin(林海军)

Fujian Provincial Key Laboratory of Optoelectronic Technology and Devices, Xiamen University of Technology, Xiamen 361024, *China*

(Received 6 August 2020; revised manuscript received 26 October 2020; accepted manuscript online 31 October 2020)

The space charge accumulation in CdZnTe crystals seriously affects the performance of high-flux pulse detectors. The influence of sub-bandgap illumination on the space charge distribution and device performance in CdZnTe crystals were studied theoretically by Silvaco TCAD software simulation. The sub-bandgap illumination with a wavelength of 890 nm and intensity of 8×10^{-8} W/cm^2 were used in the simulation to explore the space charge distribution and internal electric field distribution in CdZnTe crystals. The simulation results show that the deep level occupation faction is manipulated by the sub-bandgap illumination, thus space charge concentration can be reduced under the bias voltage of 500 V. A flat electric field distribution is obtained, which significantly improves the charge collection efficiency of the CdZnTe detector. Meanwhile, premised on the high resistivity of CdZnTe crystal, the space charge concentration in the crystal can be further reduced with the wavelength of 850 nm and intensity of 1×10^{-7} W/cm^2 illumination. The electric field distribution is flatter and the carrier collection efficiency of the device can be improved more effectively.

Keywords: CdZnTe detector, sub-bandgap illumination, space charge, charge collection efficiency

PACS: 61.72.uj, 61.72.–y, 85.25.oj, 78.56.Cd **DOI:** 10.1088/1674-1056/abc67e

1. Introduction

Cadmium zinc telluride (CdZnTe) emerges as the leading semiconductor crystals for fabricating room-temperature x-ray and gamma-ray detectors, which were widely used in nuclear medical images, non-destructive inspection, scientific x-ray and gamma-ray imaging and spectroscopy.[1–3] However, various structural defects were inevitably induced into crystals during the complex crystal growth process, which is harmful to the carrier transport process and collection seriously via carrier trapping and recombination effect.[4] Especially when the detector worked in the high counting rate mode, the accumulation of the space charge at defect levels will cause electric field distortion and thus seriously deteriorate device performance.[5–8] Therefore, it is of great importance to understand the space charge accumulation mechanisms in the cadmium zinc telluride crystals and establish a method to avoid device damage caused by the space charge accumulation effect.

In recent years, many efforts have been made to study the effect of the sub-bandgap illumination on the device performance. Alekseeva *et al.*[9] showed that the sub-bandgap illumination could regulate the occupation state of electrons and holes in the deep level, thus improving the collection efficiency of devices. Washington *et al.* also found that the sub-bandgap illumination has a significant influence on the internal electric field distribution.[10] It has been demonstrated that the sub-bandgap illumination is effective for improving the charge collection efficiency under proper illumination wavelength and power. However, the changes of deep levels occupation, space charge distribution, and their relation with the electric field distribution under the sub-bandgap illumination have not been fully established in CdZnTe detectors. Meanwhile, how to select appropriate illumination conditions to suppress the adverse effects of the space charge accumulation in crystals is a considerable interest to focus on. The Silvaco TCAD simulation technique has high simulation accuracy, which has outstanding advantages in semiconductor device performance simulations.[11–14] So in the present research, the Silvaco TCAD simulation technique is applied to simulate the space charge distribution in CdZnTe crystal before and after sub-bandgap illuminations. The influences of the sub-bandgap illumination on the defect level occupation fraction, space charge, and internal electric field distributions are investigated systematically. At the same time, the influence of sub-band gap illumination on the charge collection efficiency of detector is also discussed. The simulation results will provide some theoretical guidance for improving the collection efficiency of CdZnTe imaging devices.

*Project supported by the Young Scientists Fund of the National Natural Science Foundation of China (Grant Nos. 51702271 and 61904155) and the Natural Science Foundation of Fujian Province, China (Grant No. 2020J05239).

†Corresponding author. E-mail: 2016000050@xmut.edu.cn

© 2021 Chinese Physical Society and IOP Publishing Ltd

2. Silvaco TCAD simulation method description and model establishment

In this paper, Silvaco TCAD[15] is used to conduct (2D) numerical simulation of Au/CdZnTe/Au detectors to study the effect of the sub-bandgap illumination on the defect level occupation fraction, space charge, and internal electric field distribution in crystal. Three fundamental semiconductor equations: Poisson equation, carrier continuity equation, and current density equation are used in this paper. SRH recombination model, Auger recombination model, and optical generation/radiative recombination are applied to simulate the carrier transport processes, considering the recombination, trapping, and de-trapping effects in the simulation.

CdZnTe crystal is set as n-type semiconductor, and its specific parameters are shown in Table 1. In this simulation, a compensation model with three defect levels[16] is adopted, considering the shallow donor, shallow acceptor, and deep donor levels in crystal. The distribution of defect levels is shown in Fig. 1(b). The concentration of the shallow donor level is defined as 1.1×10^{12} cm^{-3}. And the concentration of the shallow acceptor level is defined as 1.2×10^{12} cm^{-3}. The shallow donor level and the shallow acceptor level are assumed completely ionized at room temperature. Meanwhile, it is well known that Te_{Cd}^{++} is a common deep donor level located at $E_V + 0.86$ eV[17] in the CdZnTe crystal with doped In. The specific simulation parameters of deep donor level are shown in Table 2. The sub-bandgap illumination is incident from the cathode side, as shown in Fig. 1(a). The sub-bandgap illuminations with different wavelengths and intensities are selected, and the specific simulation parameters are shown in Table 3 and Table 4. The penetration depths of sub-bandgap light with wavelength of 850 nm, 890 nm, and 940nm in CdZnTe crystal are 1.2 mm, 4.6 mm, 9.2 mm, respectively, which are larger than the thickness of the CdZnTe crystal. The non-equilibrium carriers are distributed uniformly. Thus, the diffusion effect can be ignored.[18,19]

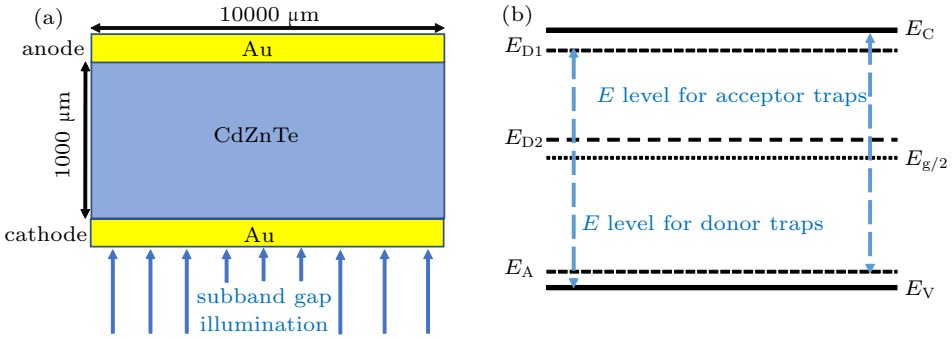


Fig. 1. (a) Au/CdZnTe/Au device structure diagram, (b) defect energy level distribution in the CdZnTe crystal.

Table 1. Basic information about CdZnTe crystals.[17,20–22]

Type	Value	Type	Value
Permittivity	10.9	Band gap/eV	1.6
Effective density of states in the conduction band at 300 K (cm^{-3})	9.14×10^{17}	Effective density of states in the valence band at 300 K (cm^{-3})	5.19×10^{18}
Electron mobility [cm^2·(V·s)$^{-1}$]	1000	Hole mobility [cm^2·(V·s)$^{-1}$]	100
Electron Auger coefficient (cm^6·s^{-1})	5×10^{-30}	Hole Auger coefficient (cm^6·s^{-1})	1×10^{-31}
Optical recombination rate (cm^3·s^{-1})	1.5×10^{-10}		

Table 2. Basic information about CdZnTe crystals.[17]

Type	Position (eV)	Concentration (cm^{-3})	Electron capture cross section (cm^2)	Hole capture cross section (cm^2)	Degeneracy
Donor	$E_V + 0.86$	1×10^{12}	3×10^{-14}	3×10^{-15}	2

Table 3. Basic parameters of illumination conditions.[5,18,19,23]

Wavelength (nm)	Extinction coefficient (k)	Refractive index (n)	Illumination intensity (W·cm^{-2})	Absorption coefficient (cm^{-1})
850	2.707×10^{-4}	2.9511	8×10^{-8}	40
890	1.417×10^{-4}	2.9196	8×10^{-8}	10
940	3.540×10^{-5}	2.8796	8×10^{-8}	5

3. Influence of sub-bandgap illumination on carrier concentration of CdZnTe crystals

To explore the influence of sub-bandgap illumination on the energy level occupation probability, the crystal is illuminated by a sub-bandgap illumination with wavelength of 890 nm and intensity of 8×10^{-8} W/cm^2. The simulation results of carrier concentration distributions in crystals before and after illumination are shown in Fig. 2.

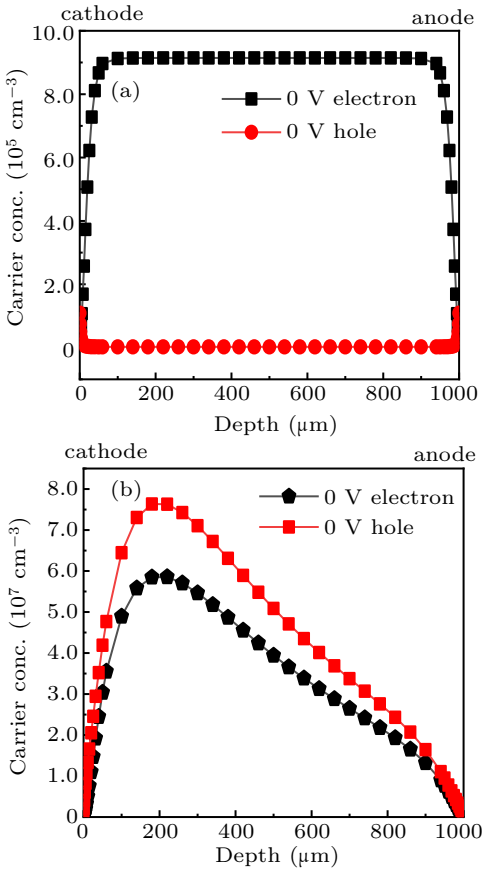


Fig. 2. Carriers concentration (conc.) distribution of crystal (a) in dark, (b) under illumination.

The carrier concentration after illumination is much higher than before. At the same time, the bulk resistivities of CdZnTe in the dark and with sub-bandgap illumination are determined to be 6.66×10^9 Ω·cm and 1.37×10^8 Ω·cm, respectively. On thermal equilibrium, Femi level is near the middle of the energy band gap in CdZnTe crystals to achieve high resistivity. However, when CdZnTe crystal was illuminated, the quasi-Fermi energy level of electrons moved up, while that of holes moved down,[24] thus the concentration of carriers in the crystal is increased. As shown in Fig. 2(b), the hole concentration increased largely in comparison with electron concentration after sub-bandgap illumination. The changes of carrier concentration and resistivity indicate that the probability of defect level occupation in the crystal is changed. The possible mechanisms of the carrier concentration changes will be discussed in the next section.

4. The influence of sub-bandgap illumination on ionized concentration of deep level and space charge distribution in crystals

The change of the carrier concentration in crystal before and after sub-bandgap illumination indicates that the occupying probability of defect level in the crystal has changed. To further understand the influence of sub-bandgap illumination on CdZnTe crystals, the ionized concentration of deep donor level is simulated under a sub-bandgap illumination irradiation with a wavelength of 890 nm and an illumination intensity of 8×10^{-8} W/cm^2. The crystal was set under 0 V, 150 V, and 500 V biases respectively. Figure 3 compares the distribution of deep donor ionization and space charge concentration of crystals under different bias voltages before and after illumination. According to Figs. 3(a)–3(c), the ionization concentration of the deep donor level decreases gradually from cathode to anode under bias. This is caused by the band tilt of Au/CdZnTe/Au structured devices under bias.[18] Figure 3(d) is the schematic diagram of MSM structure energy band of Au/CdZnTe/Au under bias without sub-bandgap illumination. As shown in Fig. 3(d), in the thermal equilibrium, the Fermi level lies above or close to the level with deep centers. The exact position of the Fermi level is dependent upon temperature and concentration of free carriers. Nevertheless, it might be considered that traps are neutral. At the metal–semiconductor (MS) interface bands are tilted due to the Schottky effect. Under biases the quasi-Fermi level is linearly sloped, intersects the deep level and gets above it. Electrons, that so far occupied in neutral centers, leave the centers empty. With the increase of applied bias voltages, the energy band tilted intensifies, thus increased the ionization probability of the deep donor. Meanwhile, as shown in Figs. 3(a)–3(c), the total concentration of ionized deep donor levels decreases under the sub-bandgap illumination. With the increase of applied biases, it is more effective in reducing the ionized concentration of the deep donor level under sub-bandgap illumination. The reason can be explained by Shockley–Read–Hall (SRH) model.[25] Six thermal and optical transition processes in this model are used to describe the transition of carriers with the deep donor level, including: electron capture (thermal emission) from (to) conduction band, hole capture (thermal emission) from (to) valence band, and optical emission of electron (hole) from defect level to conduction (valence) band, as shown in Fig. 3(e). The simulation results show that the concentration of the ionized deep donor level is reduced under the sub-bandgap illumination, *i.e.*, the occupation probability of deep donor level is increased. It may the due to the promotion of electron transition from valance band to the ionized deep donor under sub-bandgap illumination (*i.e.*, the process 6 plays the dominant

role). Thus, the active deep donor level (Te_{Cd}^{++}) turned to a neutral state (Te_{Cd}^{0}) under the sub-band gap illumination. Further, the concentration of space charge will be reduced and the electric field will turn flat. The probability of excess carriers being captured by ionized deep donor level will be reduced in the charge transport process, thus significantly increasing the charge collection efficiency of detectors, which will be discussed in the next section. On the other hand, the promotion of electron transition from valance band to the ionized deep donor under sub-bandgap illumination causes the increase of hole concentrations, which is consist with the results as shown in Fig. 2(b).

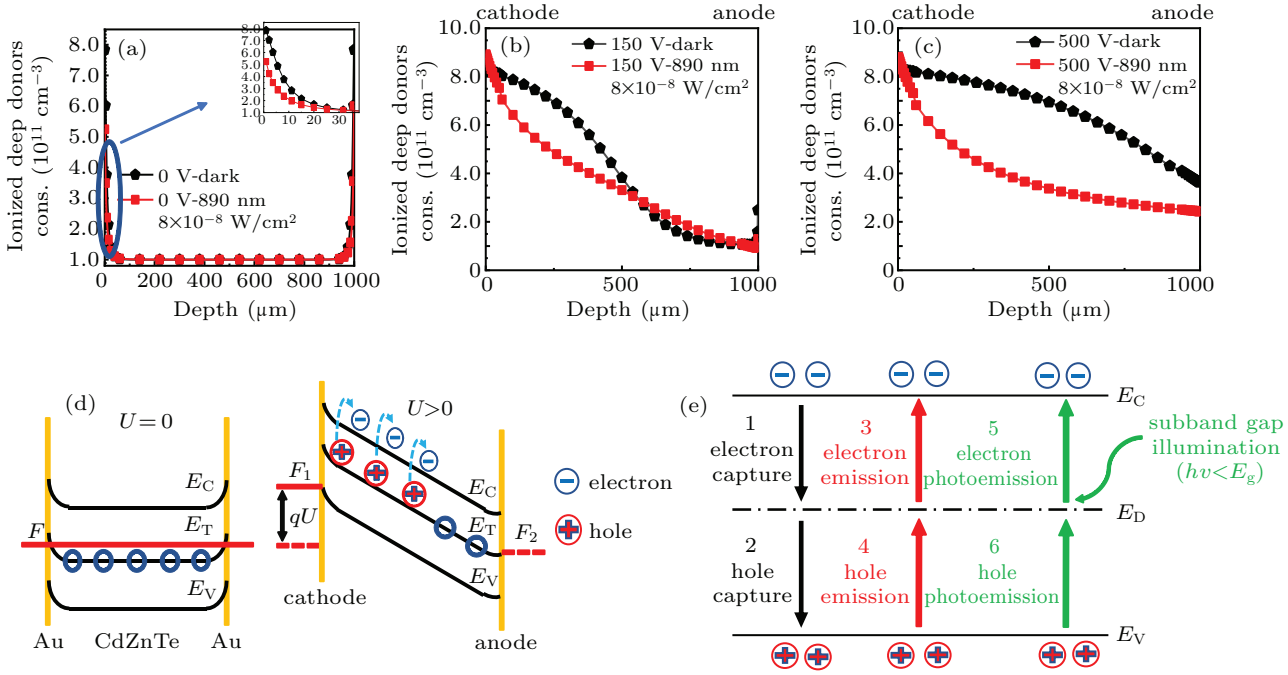


Fig. 3. Distribution of ionized deep donor level concentration (cons.) under different biases (a) 0 V, (b) 150 V, (c) 300 V before and after sub-bandgap illumination, (d) schematic diagram of MSM structure energy band under biases, (e) diagram of major processes containing a deep donor defect level in CdZnTe crystals under sub-bandgap illumination (arrow direction is the direction of electron transitions).

5. Influence of sub-bandgap illumination on internal electric field distribution and charge collection efficiency

Figure 4 shows the space charge distribution and internal electric field distribution under bias voltages of 150 V and 500 V before and after sub-bandgap illumination, respectively. The variation of space charge concentration under sub-bandgap illumination directly affects the electric field distribution in the CdZnTe crystal. The electric field distribution in the CdZnTe crystal can be calculated by Poisson equation[15]

$$-\frac{\mathrm{d}^2\varphi}{\mathrm{d}x^2}=\frac{\mathrm{d}E}{\mathrm{d}x}=\frac{\rho}{\varepsilon_s}=\frac{q}{\varepsilon_s}(p+N_{SD}^{+}+N_{DD}^{+}-n-N_{SA}^{-}), \quad (1)$$

where φ is the electrostatic potential, E is the electric field, ε_s is the dielectric constant, N_{SD}^{+} is the concentration of the ionized shallow donor level, N_{SA}^{-} is the concentration of the ionized shallow acceptor, N_{DD}^{+} is the concentration of the ionized deep donor level, n (p) is the concentration of free electrons (holes). As shown in Fig. 4, the internal electric field becomes significantly flatter under the sub-bandgap illumination with a wavelength of 890 nm and illumination intensity of 8×10^{-8} W/cm^2. As it has been discussed above, the process of electron optical excitation from valence band to the ionized deep donor level under the sub-bandgap illumination plays the dominant role in transitions. This process results in a decrease of ionized deep donor level's concentration, thus reducing the space charge concentration and flattening the electric field.

The charge collection efficiency is the ratio of the quantity of carriers received by electrodes to the total quantity of carriers generated by implying the ray into the device. To further understand the effect of electric field on charge collection efficiency with sub-bandgap illumination. The famous Hecht equation[26] is utilized to analyze the collection efficiency (CCE) of the CdZnTe detector carriers,

$$\mathrm{CCE}=\mu_e\tau_e E\left(1-\exp\left(\frac{Z-D}{\mu_e\tau_e ED}\right)\right)+\mu_h\tau_h E\left(1-\exp\left(\frac{-Z}{\mu_h\tau_h ED}\right)\right), \quad (2)$$

where μ_e and τ_e are the mobility and lifetime of electrons, respectively, and the product of which is 3×10^{-3} cm$^2\cdot$V^{-1}, μ_h and τ_h are the mobility and lifetime of the hole, respectively, and the product of which is 5×10^{-5} cm$^2\cdot$V^{-1}.[26] E is the internal electric field, which is imported by Silvaco TCAD simulation. D is the thickness of the detector which is 0.1 cm in this simulation, and Z is the position where the incident ray interacts with the crystal.

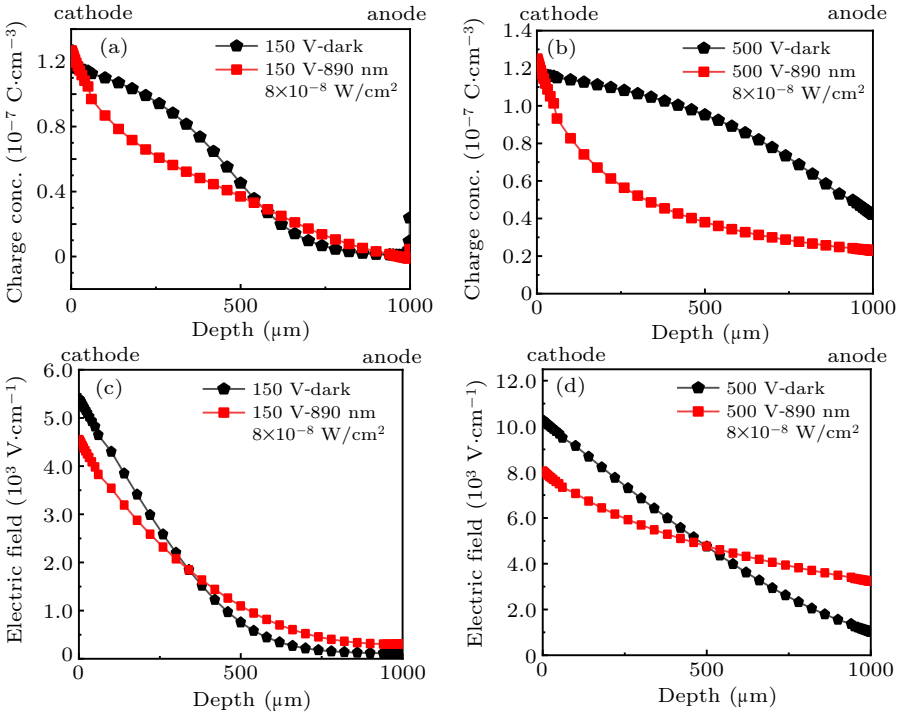


Fig. 4. (a) Space charge distribution in CdZnTe crystal under bias of 150 V, (b) under bias of 500 V, (c) internal electric field distribution of CdZnTe crystal under bias of 150 V, (d) bias of 500 V before and after sub-bandgap illuminations.

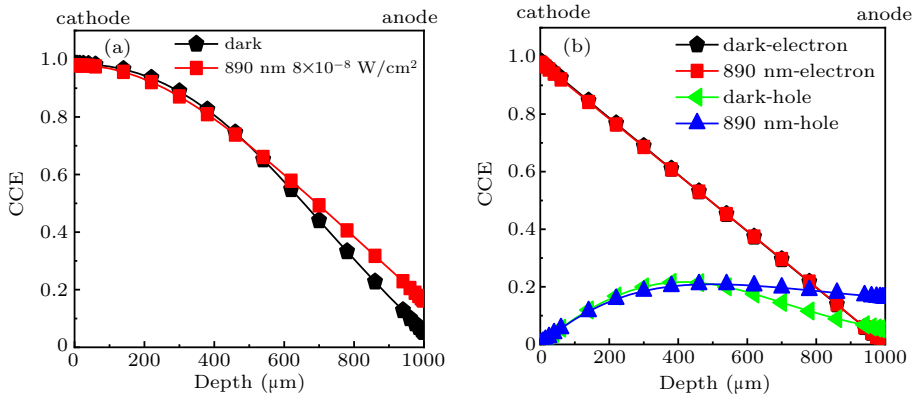


Fig. 5. CCE distribution before and after sub-bandgap illuminations: (a) total charge collection efficiency and (b) charge collection efficiency of electron and hole.

The charge collection efficiency (CCE) of electrons and holes of the CdZnTe detector is calculated by Hecht equation, as shown in Fig. 5.

As shown in Fig. 5(a), the charge collection efficiency of the detector is significantly improved under the sub-bandgap illumination, especially in the area near the anode. Meanwhile, the charge collection efficiency of holes improved more significantly than electrons, as shown in Fig. 5(b). This is mainly due to the sub-bandgap illumination, the internal electric field becomes flatten, which improves the total charge collection efficiency of the device. However, the charge collection efficiency of detector has already reached 97% at the distance of 0.01 cm from cathode without sub-band gap illumination. Thus, the improvement of detector collection efficiency under sub-bandgap illumination near the cathode is non-significant.

6. The influence of sub-bandgap illumination with different conditions on space charge distribution and charge collection efficiency

The simulation results of the resistivity of CdZnTe crystal under different sub-bandgap illuminations are shown in Table 4. It can be seen that with the increase of illumination intensity, the resistivity decreases gradually. When the illumination intensity is 5×10^{-7} W/cm^2, the resistivity is as low as the value of 2.89×10^7 Ω·cm. In this section, on the premise of ensuring high resistance of crystals, three different wavelengths of sub-bandgap illumination (number 1–3) and six different illumination intensities of sub-bandgap illumination (number 3–7) are selected to explore their influence on ionized concentration, space charge, and internal electric field distribution of CdZnTe crystals.

Table 4. Resistivity of CdZnTe crystal under different sub-bandgap illuminations.

Number	Wavelength (μm)	Illumination intensity ($W\cdot cm^{-2}$)	Resistivity ($\Omega\cdot cm$)
1	940	8×10^{-8}	2.58×10^{8}
2	890	8×10^{-8}	1.37×10^{8}
3	850	8×10^{-8}	1.76×10^{8}
4	850	3×10^{-9}	2.81×10^{9}
5	850	1×10^{-8}	1.92×10^{9}
6	850	4×10^{-8}	3.44×10^{8}
7	850	1×10^{-7}	1.42×10^{8}
8	850	5×10^{-7}	2.89×10^{7}

6.1. Effects of sub-bandgap illumination with different wavelengths on space charge distribution and charge collection efficiency

In order to further understand the influence of sub-bandgap illumination on the ionized concentration, space charge, and internal electric field distribution in crystals. In this section, the wafer is irradiated under three different wavelengths of 850 nm, 890 nm, and 940 nm, respectively, with the illumination intensity of 8×10^{-8} W/cm^2. The relevant ionized concentration, space charge, internal electric field distribution, and charge collection efficiency obtained at bias voltage of 500 V are shown in Fig. 6. It can be seen that, the ionized concentration of deep donor level under 850-nm illumination is significantly lower than that under 890-nm and 940-nm illuminations. And the space charge concentration under 850-nm illumination is lower, either, which results in a flatter internal electric field and more effectively improving charge collection efficiency of the detector. The simulation results correspond to the experimental results of Cola.[5]

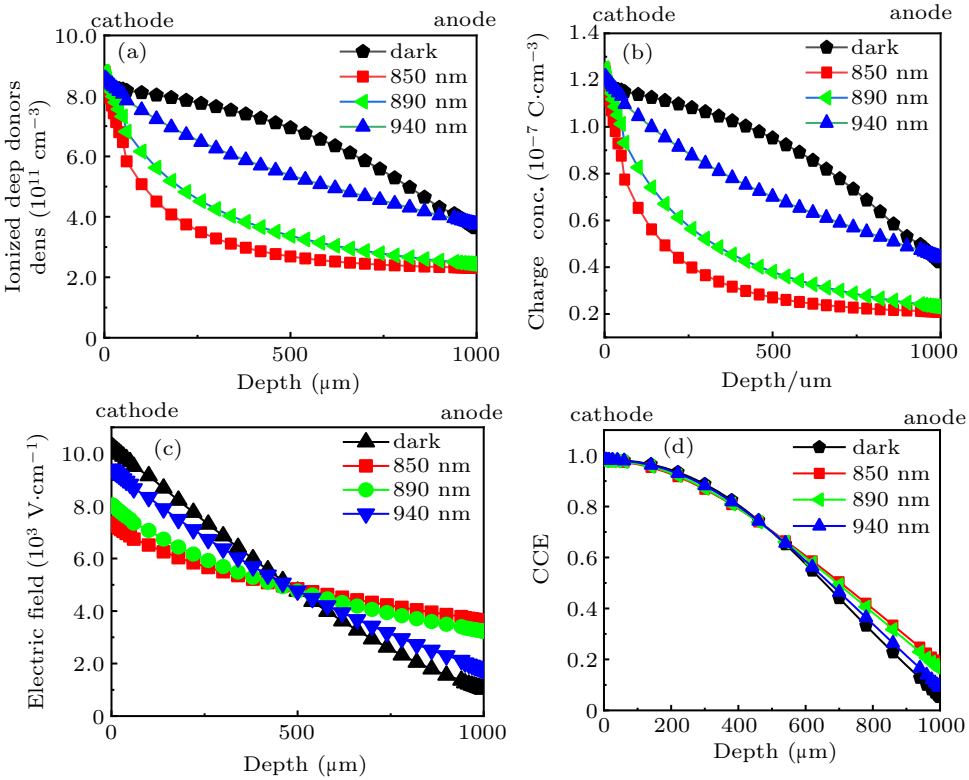


Fig. 6. (a) Distribution of ionized deep donor level concentration (conc.), (b) space charge concentration, (c) internal electric field, (d) charge collection efficiency under different subbandgap wavelengths and 500 V bias.

6.2. Effects of sub-bandgap illumination with different illumination intensities on space charge distribution and charge collection efficiency

The influences of different wavelengths on space charge distribution and charge collection efficiency have been investigated in the previous section. The simulation shows that the charge collection efficiency can be improved more effectively under the sub-bandgap illumination of 850 nm. Based on Table 4, the resistivity of the crystal decreases with increasing illumination intensity. When the illumination intensity is 5×10^{-7} W/cm^2 at wavelength of 850 nm, the resistivity of crystal reaches as low as 10^7 Ω·cm. To avoid introducing excessive leakage current due to illumination, different illumination intensities (3×10^{-9} W/cm^2, 1×10^{-8} W/cm^2, 8×10^{-8} W/cm^2, 4×10^{-8} W/cm^2, 8×10^{-8} W/cm^2, and 1×10^{-7} W/cm^2) under the bias voltage of 500 V and the wavelength of 850 nm are selected to simulate the ionized deep donor concentration distribution, space charge, internal electric field, and charge collection efficiency in crystals. The corresponding results are shown in Fig. 7. As shown in Fig. 7, different illumination intensities have different effects on the occupation probability of defect level in crystals. When the

illumination intensity is 3×10^{-9} W/cm^2, the ionized deep donor level concentration (at the same position of the crystal) is significantly higher than that under other conditions. The larger ionization concentration of deep donor level, leads to an increase of space charge concentration in the crystal, which makes the internal electric field even more uneven. Therefore, it is detrimental to the charge collection of detectors. With the increase of illumination intensity, the concentration of ionized deep donor level decreases. When the illumination intensity increased to 1×10^{-7} W/cm^2, the concentration of the ionized deep donor level at the same position in the crystal is greatly reduced, thus reducing the concentration of space charge and making the internal electric field flattening. As shown in Fig. 7(d), when the illumination intensity is 1×10^{-7} W/cm^2, the carrier collection efficiency at the anode position of the detector is significantly improved therefore, it is more effective in improving the overall charge collection of detectors.

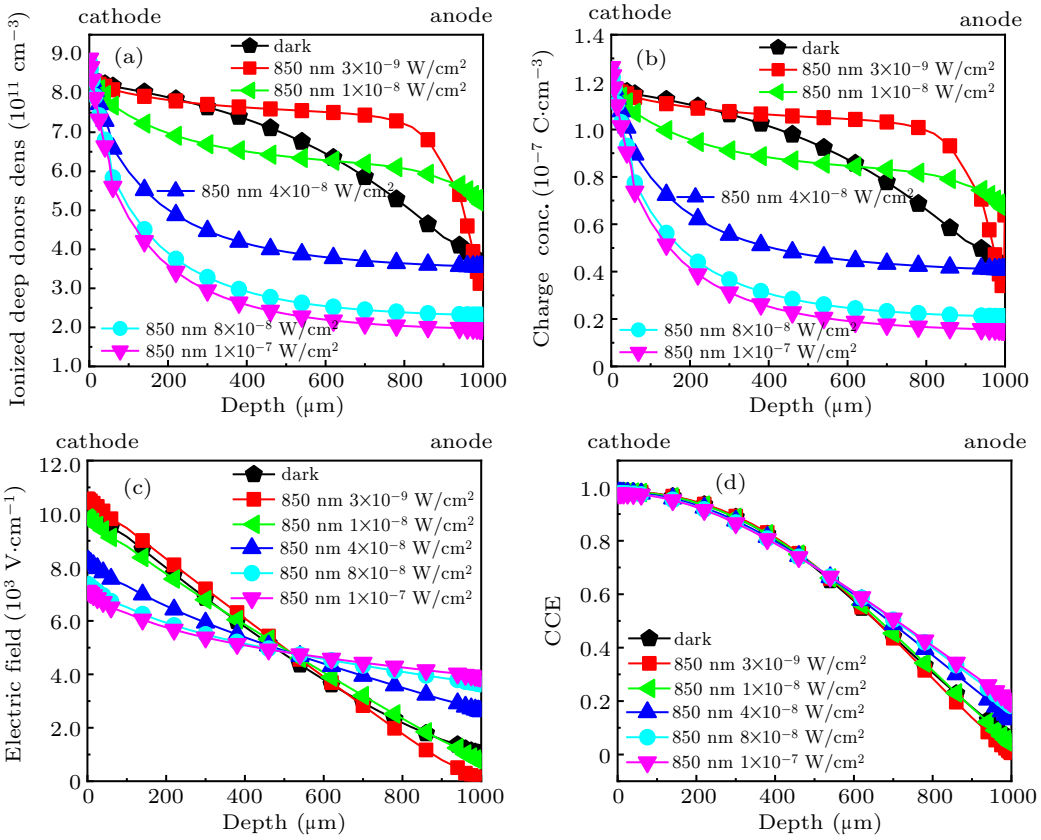


Fig. 7. (a) The distribution of ionized deep donor level concentration, (b) space charge concentration, (c) internal electric field, (d) carrier collection efficiency in the crystal under bias of 500 V, wavelength of 850 nm with different illumination intensities.

7. Conclusions

In this paper, the effects of sub-bandgap illumination on the space charge distribution, internal electric field distribution, and charge collection efficiency of CdZnTe detector are simulated using the semiconductor device simulation software named Silvaco TCAD. The simulation results show that, under sub-bandgap illumination with wavelength of 890 nm and light intensity of 8×10^{-8} W/cm^2, the sub-bandgap illumination promotes optical excitation of electrons from the valence band into the ionized deep donor levels (located in $E_V+0.86$ eV with concentration of 1×10^{12} cm $^{-3}$). A neutral state of deep donor level is formed due to the increasing probability of deep donor levels being occupied by electrons. Thus, the space charge concentration is reduced in the crystal and the internal electric field turns to flat under the sub-band gap illumination. Therefore, the charge collection efficiency of the detector is significantly improved. When the wavelength of sub-bandgap illumination is 850 nm, the concentration of the ionized deep donor level and space charge at the same position of the crystal can be further reduced, thus making the internal electric field flatter. At this time, ensuring the CdZnTe crystal with high resistivity, enhancing the light intensity to 1×10^{-7} W/cm^2 can also reduce the concentration of the ionized deep donor level and space charge. This results in a flatter internal electric field, which greatly reduces the probability of carriers being trapped or recombined by defect levels during charge transport processes and then significantly improves the charge collection efficiency of detectors.

Acknowledgment

The authors would like to give special thanks to Dr. Tao Wang from Northwestern Polytechnical University for the

fruitful discussion during the writing of this paper.

References

[1] Czyz S A, Farsoni A T and Gadey H R 2019 *Nucl. Instrum. Methods Phys. Res. Sect. A* **945** 162614

[2] Guo Q, Beilicke M, Garson A, Kislat F, Fleming D and Krawczynski H 2012 *Astropart. Phys.* **41** 63

[3] Johns P M and Nino J C 2019 *J. Appl. Phys.* **126** 040902

[4] Bolotnikov A E, Babalola S, Camarda G S, *et al.* 2011 *IEEE Trans. Nucl. Sci.* **58** 1972

[5] Cola A and Farella I 2013 *Sensors (Basel)* **13** 9414

[6] Musiienko A, Grill R, Pekárek J, Belas E, Praus P, Pipek J, Dědič V and Elhadidy H 2017 *Appl. Phys. Lett.* **111** 082103

[7] Mahmood S A 2019 *J. Appl. Phys.* **125** 214505

[8] Thomas B, Veale M C, Wilson M D, Seller P, Schneider A and Iniewski K 2017 *J. Inst.* **12** C12045

[9] Alekseeva L, Dorogov P, Ivanov V, Loutchanski A, Grigorjeva L and Millers D 2012 *IEEE Nuclear Science Symposium Conference Record,* Valencia, Spain, 23–29, October, 2011, p. 4562

[10] Washington A L, Teague L C, Duff M C, Burger A, Groza M and Buliga V 2011 *J. Appl. Phys.* **110** 073708

[11] Ellakany A A, Abouelatta M, Shaker A, Sayah G T and El-Banna M 2017 *J. Eng.* **2017** 574

[12] Maneuski D, Gostilo V and Owens A 2019 *J. Phys. D: Appl. Phys.* **53** 015114

[13] Das A, and Duttagupta S P 2015 *Radiat. Prot. Dosim.* **167** 443

[14] Johannesson D, Nawaz M and Nee H P 2019 *Mater. Sci. Forum.* **963** 670

[15] Tang L G 2014 *Semiconductor process and device simulation software Silvaco TCAD practical tutorial* (Beijing: Tsinghua University Press) p. 99 (in Chinese)

[16] Prokesch M and Szeles C 2007 *Phys. Rev. B* **75** 245204

[17] Gul R, Roy U N and James R B 2017 *J. Appl. Phys.* **121** 115701

[18] Cola A, Farella I and Anni M 2012 *IEEE Trans. Nucl. Sci.* **59** 4604

[19] Montmorillon L A D, Delaye P, Launay J C and Roosen G 1995 *Opt. Mater.* **4** 233

[20] Wang N, Jie W Q, Xu L, Zha G Q and Wang T 2013 *IEEE Nuclear Science Symposium and Medical Imaging Conference*, 27 October–2 November, 2013, Seoul, South Korea, pp. 1–5

[21] Zha G Q, Wang T, Xu Y D and Jie W Q 2013 *Physics* **42** 862 (in Chinese)

[22] http://www.silvaco.com/

[23] Marple D T F 1964 *J. Appl. Phys.* **35** 539

[24] Cheng Z, Delahoy A E, Su Z and Chin K K 2014 *Thin Solid Films* **558** 391

[25] Hsieh Y K and Card H C 1989 *J. Appl. Phys.* **65** 2409

[26] Matthew C Veale 2009 *Charge Transport and Low Temperature Phenomena in Single Crystal CdZnTe* (Guildford: University of Surrey)